The effect of moisture on the nonlinearly viscoelastic behavior of an epoxy

**Daniel Ferreira Vieira de Mattos[1,2] · Rui Huang[1] ·
Kenneth M. Liechti[1]**

© Springer Nature B.V. 2020

Abstract The shear and bulk relaxation moduli required to characterize a homogeneous, isotropic, and linearly viscoelastic material were determined using a confined compression experiment and by introducing a new iterative scheme that accounts for the fact that the hoop and radial strains are not step functions. In addition, the coefficients of thermal and hygral expansion of the epoxy being considered were determined along with its diffusive behavior. Fickian diffusion of moisture was confirmed by coupling radial diffusion in an epoxy disk with optical interference measurements of the out-of-plane displacements. These properties are essential components of the modified free-volume model of nonlinear viscoelasticity established by Popelar and Liechti (J. Eng. Mater. Technol. 119:205–210, 1997, Mech. Time-Depend. Mater. 7(2):89–141, 2003). For the nonlinear component of the model, its distortional parameters were evaluated from Arcan pure shear test results at one strain rate and temperature/humidity state. The nonlinear viscoelasticity model was then used to predict the shear stress-strain response under other conditions. The dilatational parameters were extracted from uniaxial tensile test results at one strain rate and temperature humidity state and predictions under other conditions compared favorably with the results from experiments. This exercise adds to a growing list of glassy polymers whose nonlinear stress-strain behavior can be modeled by this modified free-volume model.

Keywords Linear viscoelasticity · Shear and bulk relaxation modulus · Diffusion · Thermal and hygral expansion · Nonlinear viscoelasticity · Modified free-volume model

✉ K.M. Liechti
kml@mail.utexas.edu

[1] Research Center for the Mechanics of Solids, Structures and Materials, Department of Aerospace Engineering and Engineering Mechanics, The University of Texas at Austin, Austin, TX 78712, USA

[2] Present address: Aircraft Structures Department, Aeronautics and Space Institute, Brazilian Air Force, São José dos Campos, Sao Paulo, Brazil

1 Introduction

The emphasis of this paper is on the nonlinearly viscoelastic behavior of an epoxy. The literature dealing with research in nonlinear viscoelasticity is extensive. The approaches can be broadly divided into those that result in differential or integral equations (Drozdov 1988). The focus here is on the latter. Nonlinear strain functions were introduced in the linear viscoelastic constitutive equations (Guth et al. 1946) to describe the nonlinear viscoelastic behavior of rubber. Makhmutov et al. (1983) and Viktorova (1983) decomposed the integral kernel in two parts, thereby establishing a connection with plastic effects and damage accumulation. A universal nonlinear model was formulated by Schapery (1964, 1965, 1969, 1981) assuming that the nonlinear, stress-dependent behavior of a material may be characterized in a manner following the traditional temperature superposition approach used for linear viscoelasticity where the applied stress or strain compresses or expands the material time scale. The concept of reduced time to include the nonlinearity into the integration kernel was established by Leaderman (1943). Doolittle (1951) later related the reduced time to free-volume concepts. He established that the viscosity of liquid normal paraffins can be accurately defined as a simple function of the relative free space or free volume in the material. The contribution of mechanical dilatation to the free volume was included by Fillers and Tschoegl (1977) and later by Knauss and Emri (1981) in a more explicit manner. The underlying assumption is that the free volume controls the molecular mobility, directly affecting the time scale of the material. The influence of solvent concentration on the free volume effect was established by Knauss and Kenner (1980) in a consistent manner. The model was then adapted by Losi and Knauss (1992) to describe polymer behavior above and below the glass transition temperature. A thermodynamic equation of state was used by Lustig et al. (1996) to establish the interrelation between temperature, specific volume, and mechanical dilatation. At this point in time, free-volume models were based entirely on dilatational effects and were unable to account for nonlinear behavior in shear. Although the physical basis for including distortional effects has not yet been established at molecular scales, including the distortional strain in the free volume (Popelar and Liechti 1997, 2003) did allow nonlinear effects to be accounted for in pure shear and also in cases where tension and compression were combined with shear. The possibility of stress, rather than strain, driving the nonlinear behavior of a urethane through the Tait equation was considered by Arzoumanidis and Liechti (2003). The strain-based formulation provided a better description of the nonlinear behavior of the material in monotonic and cyclic loading, although improvements are still required for cyclic loading. To include extraordinarily strong hygrothermal effects on the behavior of a urethane adhesive, Park et al. (2004) adopted a hybrid nonlinear viscoelastic constitutive model that combined the nonlinearities introduced by Schapery's models with those of the modified free-volume approach. Caruthers et al. (2004) formulated a thermodynamically consistent model based on the Helmholtz free energy for isotropic, thermorheologically simple, glassy polymers. It was validated for four amorphous polymers in a companion paper by Adolf et al. (2004) and is currently the most versatile model of the nonlinearly viscoelastic thermomechanical behavior of glassy polymers (Medvedev and Caruthers 2017). Nonetheless and because the present study began in 2014 with an emphasis on the effect of moisture concentration, the approach developed by Popelar and Liechti (1997, 2003) and refined by Park et al. (2004) was adopted in the present study.

Since the approach is based on linearly viscoelastic behavior, the paper first describes the use of the confined compression configuration to characterize the epoxy in terms of its bulk

and shear relaxation moduli. The paper follows with a description of the steps that were taken to determine the parameters for and validate the model of nonlinear viscoelasticity, including the effects of strain rate, temperature, and humidity.

2 Linearly viscoelastic behavior

Tschoegl et al. (2002) established a standard protocol requiring that the basic viscoelastic functions be determined simultaneously on the same specimen, under the same environmental conditions. The confined compression configuration was employed in the present study to satisfy this requirement.

Specimens The specimens used in the present study were made of an epoxy that consists of a primer resin (Araldite GY 505) and hardener (Aradur 955-2) mixed with a 100:35 weight ratio. After the components were mixed, bubbles were removed under cyclic vacuuming to break down the foam that was formed on the surface during the procedure. This process takes an average of half an hour. Any remaining bubbles on the surface were removed by heating the epoxy at 60 °C before pouring it into each mold. The molds were made of steel. They were cleaned using ethyl alcohol and delicate task wipers. Compressed gas was used to remove any dust and lint. The surface was then covered by a thin layer of mold release made specifically for epoxies. The epoxy was poured into the molds and cured at 100 °C for two hours. Next, the molds were cooled to room temperature, ∼20 °C, and the cured epoxy was removed from the mold and machined to make sure that the top and bottom surfaces were planar and perpendicular to the longitudinal axis.

Confined compression test The confined compression test satisfies all requirements established in the standard protocol in that two viscoelastic functions, the bulk $\kappa(t)$ and shear $\mu(t)$ relaxation moduli, can be determined in a single experiment. The epoxy was cured in a cylinder with a larger diameter than the one to be used in the test because it had been noted that there was considerable shrinkage following cure that left a gap between the cylinder and specimen. The sample was then placed in a confining cylinder (Fig. 1a) that provided a snug fit. The inside surface of this cylinder was also honed with a view to minimizing friction between the specimen, top plunger, and the confining cylinder. The dimensions of the confining cylinder were selected to minimize friction effects (Ma and Ravi-Chandar 2000) and to satisfy the requirements for Lame's solution for pressurized, thick-walled cylinders to be valid and to provide sufficient space to ensure that the strain gages on the outer surface of the confining cylinder were sufficiently removed from the ends. Two 350 Ω, diametrically opposed strain gages were attached to the confining cylinder to measure the hoop strain. A piston is placed (Fig. 1b) on the top of the specimen. Its diameter is 25 μm less than the inner diameter of the confining cylinder, which provides smooth sliding throughout as the displacement is prescribed. A plug was placed below the specimen. It has the same diameter as the piston and prevents mushrooming of the specimen. The axial, end-to-end displacement of the specimen was measured by two linearly variable differential transformers (LVDT). The use of two displacement sensors and two strain gages allowed any bending effects due to misalignment to be checked for and minimized. The displacement sensors also provided a more accurate measurement of the prescribed displacement than relying on the actuator displacement.

The test was performed in a servo hydraulic testing machine (MTS 252) using a controller (Instron model 8500). The global axial displacement and load were acquired from
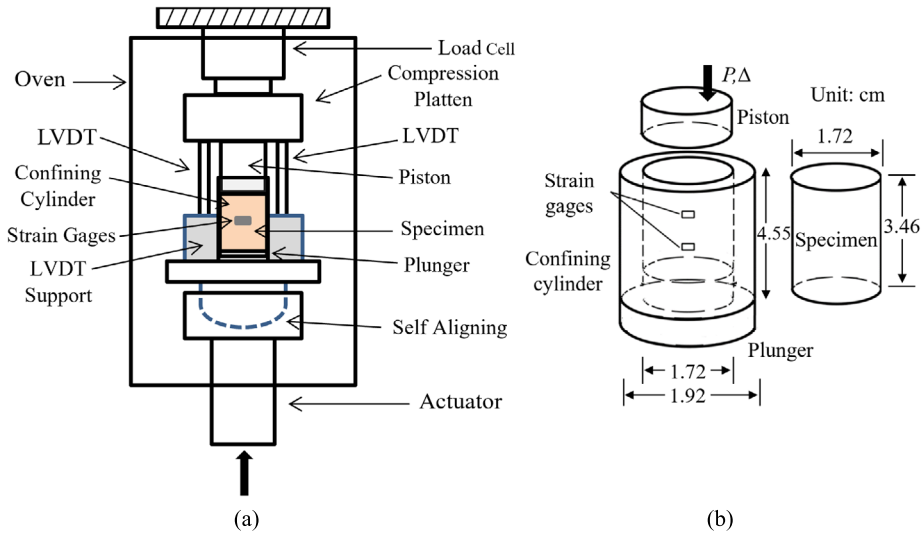
Fig. 1 (**a**) Schematic of the confined compression experiment; (**b**) detail of the specimen, confining cylinder, top piston, and bottom plunger

this controller. A displacement corresponding to an axial strain of 1.2% was prescribed using compression platens. These provide hardened surfaces (Rockwell HRC 58/60) that apply a uniform stress distribution. The bottom platen was equipped with a universal joint to assure proper alignment. The load was measured using a 9-kN load cell. The strain gages were conditioned using a Vishay Micro-measurement® amplifier. The bridge was balanced and provided a sensitivity of 0.00025 strain/volt. The LVDTs were excited and conditioned using a Sensotec® module. All conditioners were connected to an acquisition board (National Instruments®, model BNC-2090), and their signals were recorded using a LabView© application developed for this test.

All tests were conducted in a temperature-controlled chamber surrounding the specimen, which maintained the selected temperature to within ±0.5 °C. Since the confining cylinder acted as a heat reservoir, the sample temperature was even more closely controlled. The target temperature was checked by placing a thermocouple attached to dummy sample inside the chamber. A bare strain gage was used to track and compensate for any temperature effects.

The axial stress σ_{zz} was determined from the measurements from the load cell and the cross-section area of the epoxy cylinder. The axial strain ε_{zz} was determined from the displacement Δ measured by the LVDTs and the specimen length L. The hoop strain $\varepsilon_{\theta\theta}(r_0)$ measurements from the two strain gages attached on the external surface ($r = r_0$) of the confining cylinder are related to the radial and hoop stresses ($\sigma_{rr}, \sigma_{\theta\theta}$) and strains ($\varepsilon_{rr}, \varepsilon_{\theta\theta}$) in the sample using Lame´s solution for a hollow, thick-walled elastic cylinder. The normal stresses and strains are given by (Ma and Ravi-Chandar 2000):

$$\sigma_{rr} = \sigma_{\theta\theta} = -\frac{E_c}{2}\left(\frac{r_o^2}{r_i^2} - 1\right)\varepsilon_{\theta\theta}(r_o), \tag{1}$$

$$\sigma_{zz} = -\frac{P}{\pi r_i^2}, \tag{2}$$
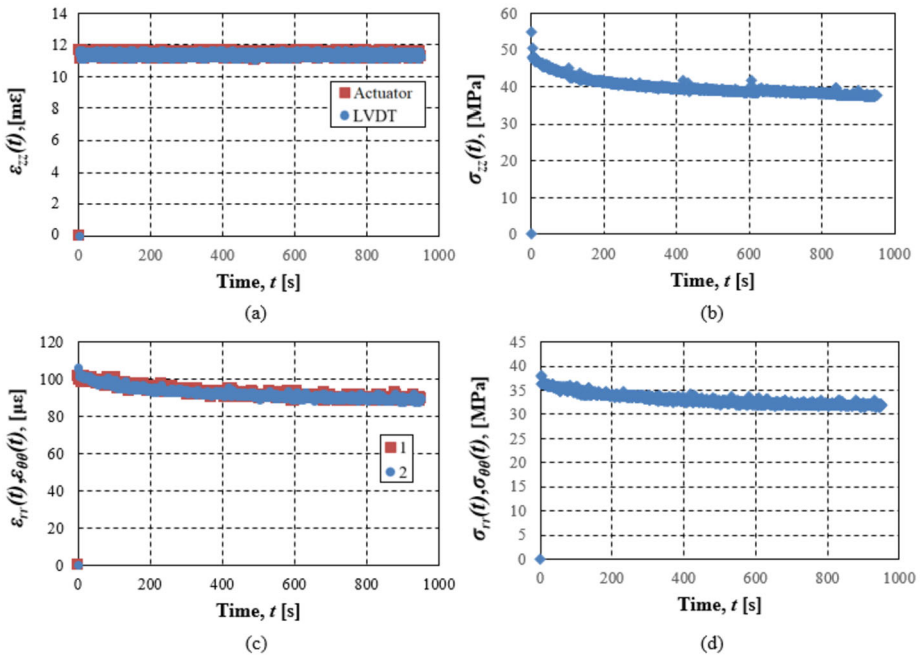
Fig. 2 Typical time history data obtained from the confined compression test: (**a**) axial strain from actuator displacement and LVDTs; (**b**) axial stress from the load cell; (**c**) radial and hoop strain; and (**d**) radial and hoop stresses from both hoop strain gages on the confining cylinder (Color figure online)

$$\varepsilon_{rr} = \varepsilon_{\theta\theta} = \frac{1}{2}\left[(1 - v_c) + (1 + v_c)\frac{r_o^2}{r_i^2}\right]\varepsilon_{\theta\theta}(r_o), \tag{3}$$

and

$$\varepsilon_{zz} = \frac{\Delta}{L}, \tag{4}$$

where E_c and v_c are the Young's modulus and Poisson's ratio of the confining cylinder, and the shear stresses and strains are zero. Consequently, there is sufficient information to determine the shear and bulk relaxation moduli, starting from the deviatoric and dilatational stress-strain relations

$$s_{ij}(t) = 2\int_0^t \mu(t - \xi)\frac{\partial e_{ij}}{\partial \xi}\,d\xi, \tag{5}$$

where $e_{ij}(t) = \varepsilon_{ij}(t) - \delta_{ij}\varepsilon_{kk}/3$ and

$$\sigma_{kk}(t) = 3\int_0^t \kappa(t - \xi)\frac{\partial \varepsilon_{kk}(\xi)}{\partial \xi}\,d\xi. \tag{6}$$

Figure 2 shows a typical data set measured from the confined compression experiment. The axial strain obtained from the displacements measured by LVDT and actuator displacement were within 1.2%. The hoop strain was below 0.1%, thereby ensuring linearly elastic behavior in the confining cylinder.

The prescribed axial strain is well represented by the Heaviside step function $\varepsilon_{zz}(t) = \varepsilon_{zz}^0 H(t)$. However, as the data in Fig. 2 indicate, the hoop and radial strains cannot be expressed as step functions. Thus the dilatational and axial distortional stresses are obtained from Eqs. (5)–(6) as

$$\sigma_{kk}(t) = 3\kappa(t)\varepsilon_{zz}^0 + 6\int_0^t \kappa(t-\xi)\frac{\partial \varepsilon_{rr}(\xi)}{\partial \xi}\, d\xi \qquad (7)$$

and

$$s_{zz}(t) = \frac{4}{3}\left[\mu(t)\varepsilon_{zz}^0 - \int_0^t \mu(t-\xi)\frac{\partial \varepsilon_{rr}(\xi)}{\partial \xi}\, d\xi\right] \qquad (8)$$

The unknown bulk and shear relaxation moduli in Eqs. (7)–(8) were determined iteratively from

$$\kappa^{i+1}(t) = \frac{\sigma_{kk}(t)}{3\varepsilon_{zz}^0} - \frac{2}{\varepsilon_{zz}^0}\int_0^t \kappa^i(t-\xi)\frac{\partial \varepsilon_{rr}(\xi)}{\partial \xi}\, d\xi \qquad (9)$$

and

$$\mu^{i+1}(t) = \frac{3}{4}\frac{s_{zz}(t)}{\varepsilon_{zz}^0} + \frac{1}{\varepsilon_{zz}^0}\int_0^t \mu^i(t-\xi)\frac{\partial \varepsilon_{rr}(\xi)}{\partial \xi}\, d\xi, \qquad (10)$$

with initial guesses obtained by considering the radial strain to be a step function, so that

$$\kappa^0(t) = \frac{\sigma_{kk}(t)}{3\varepsilon_{zz}^0 + 6\varepsilon_{rr}^0} \quad \text{and} \quad \mu^0(t) = \frac{3}{4}\frac{s_{zz}(t)}{(\varepsilon_{zz}^0 - \varepsilon_{rr}^0)}.$$

This is a more rigorous scheme for handling the fact that the radial and hoop strains were not step functions. The resulting bulk relaxation and shear relaxation master curves for reference conditions of 20 °C and 55% RH are presented in Fig. 3, where the inset indicates that only three iterations were required to reach convergence. The results from the individual tests that were run at 20 °C, 26.4 °C, 29.5 °C, 35 °C, 40 °C, 45 °C, 50 °C, 55 °C, 60 °C, and 70 °C and led to the master curve shown in the Appendix. The master curves were constructed by application of the time-temperature-superposition principle. The bulk modulus did not change much, with a glassy and rubbery moduli of 5.78 and 2.96 GPa, respectively, and a two-decade transition. The glassy shear modulus was 1.16 GPa and transitioned to a rubbery modulus of 7.67 MPa over 8 decades in time.

The glass transition temperature was measured using a dynamic mechanical analyzer (RSA G2). A strip of neat epoxy measuring $50 \times 5 \times 1$ mm in length, width, and thickness was placed in three-point bending inside a temperature chamber. The temperature was increased from 21 to 85 °C at a rate of 1 °C/min to allow for thermal equilibrium. The specimen was subjected to 1-Hz frequency and 0.1% strain amplitude. All test parameters were controlled and acquired by Trios© software. The storage and loss moduli and loss tangent are shown in Fig. 4, where the glass transition temperature is seen to be 40 °C at the maximum value of the loss tangent.

The evaluated viscoelastic functions were fitted and expressed as the Prony series representation forms

$$\kappa(t) = \kappa_\infty + \sum_{i=1}^N \kappa_i e^{-t/\tau_i} \qquad (11)$$
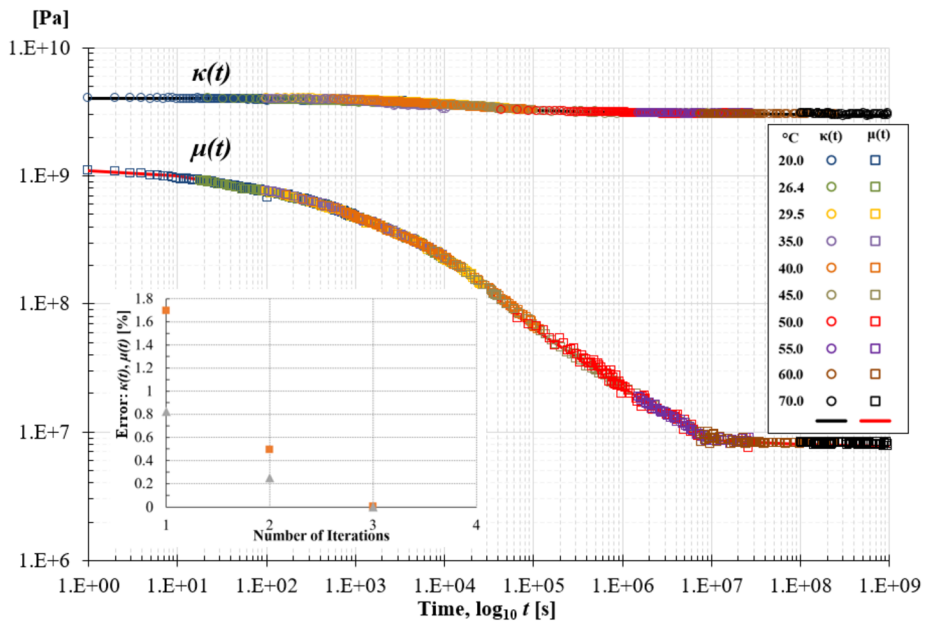
Fig. 3 Bulk $\kappa(t)$ and shear $\mu(t)$ relaxation moduli of the epoxy (Color figure online)
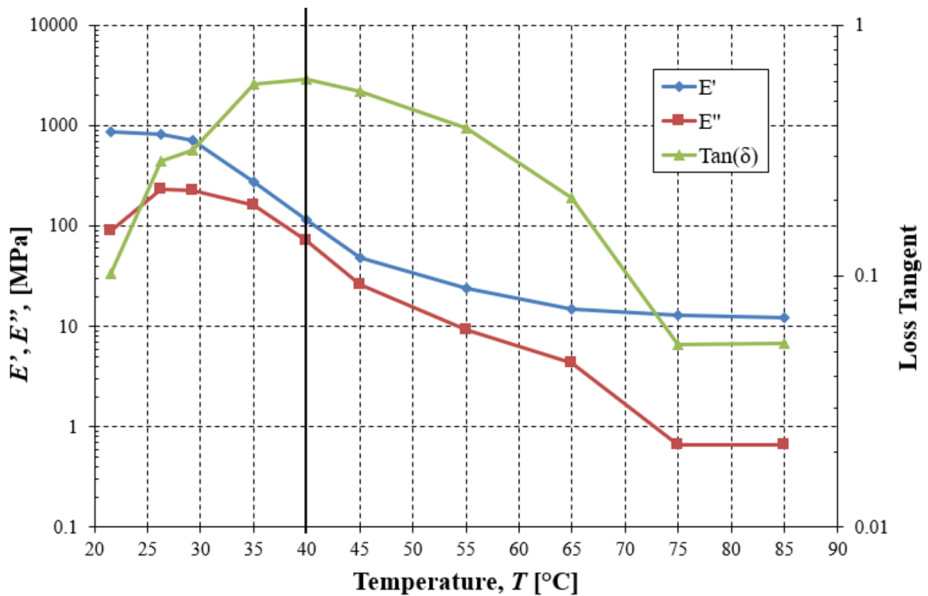
Fig. 4 Determining the glass transition temperature (40 °C) of the epoxy using the loss tangent

and

$$\mu(t) = \mu_\infty + \sum_{i=1}^{n} \mu_i e^{-t/\tau_i}, \qquad (12)$$
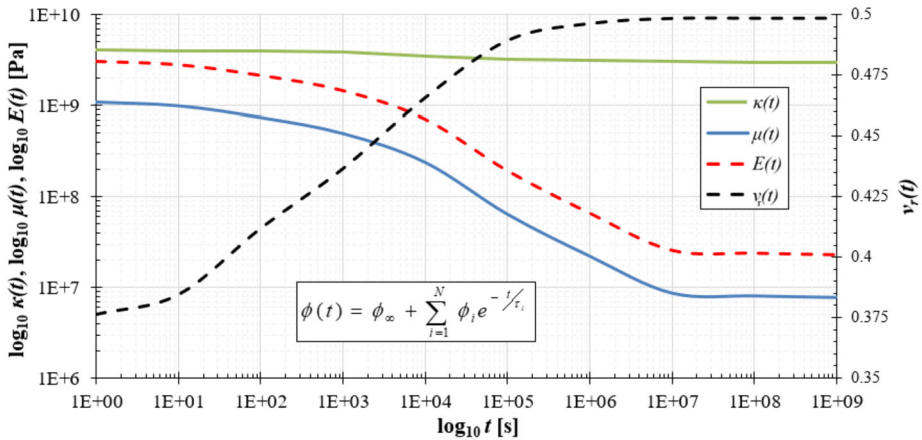
Fig. 5 Prony series representations of the bulk and shear relaxation moduli of the epoxy (solid lines) along with those of the tensile relaxation modulus and Poisson's ratio in relaxation (dashed lines)

where κ_∞ and μ_∞ are the bulk and shear equilibrium moduli, respectively. The challenge is finding the parameters $(\kappa_i, \mu_i, \tau_i)$ that provide a good fit over the time span of the data. This problem has been addressed by several methods in the literature including an approach that is attributed to Tobolsky and Murakami in (Tschoegl 2012), the collocation method by Schapery (1962), which was adopted in this work, the multidata method (Cost and Becker 1970), the windowing method (Emri and Tschoegl 1993), and the sign control method developed by Bradshaw and Brinson (1997).

Interconversion The measured shear and bulk relaxation moduli were used to determine the tensile relaxation modulus $E(t)$ and Poisson's ratio in relaxation $v_r(t)$ of the epoxy, as these are required for determining some of the parameters of the modified free volume model. In the Carson transform domain,

$$\tilde{E}(s) = \frac{9\tilde{\mu}(s)\tilde{\kappa}(s)}{\tilde{\mu}(s) + 3\tilde{\kappa}(s)} \tag{13}$$

and

$$\tilde{v}_r(s) = \frac{3\tilde{\kappa}(s) - 2\tilde{\mu}(s)}{2[\tilde{\mu}(s) + 3\tilde{\kappa}(s)]}, \tag{14}$$

where $\tilde{f}(s) = s \int_0^\infty f(t)e^{-st}\,dt$ is the Carson transform of the function $f(t)$, and s is the transform parameter. The deduced functions in the transformed domain were inverted to the time domain by using Schapery's direct approximate method (Schapery 1962). The resulting relaxation functions were also fitted by Prony series. Figure 5 presents the fits to the bulk and shear relaxation data along with the deduced functions for the tensile relaxation modulus and Poisson's ratio in relaxation. The Prony series coefficients for all four functions are provided in Table 1.

Tensile relaxation test A series of tensile relaxation tests were used to determine the tensile relaxation modulus as check on the interconversion procedure. The tests were performed in a Dynamical Mechanical Analyzer (RSA G2) with a series of constant temper-

log(τ_i) [s]	τ_i [s]	κ_i [Pa]	μ_i [Pa]	E_i [Pa]	ν_i
0	1	2.17E+08	7.58E+07	2.57E+08	−2.51E-03
1	1E+1	1.60E+06	6.95E+07	1.08E+08	−6.11E-03
2	1E+2	2.11E+08	3.90E+08	1.07E+09	−4.50E-02
3	1E+3	2.60E+07	1.37E+08	3.50E+08	−7.48E-03
4	1E+4	5.76E+08	3.80E+08	1.10E+09	−4.74E-02
5	1E+5	1.54E+08	6.20E+07	1.88E+08	−1.07E-02
6	1E+6	8.65E+06	3.56E+07	1.07E+08	−5.64E-03
7	1E+07	6.58E+07	4.45E+05	1.40E+06	−6.40E-05
8	1E+08	1.11E+08	7.63E+05	2.28E+06	−8.08E-05
9	1E+09	2.16E+06	5.43E+04	1.63E+05	−8.58E-06
∞		2.96E+09	7.67E+06	2.30E+07	0.4987

Table 1 Prony series coefficients

atures that ranged from 20 to 85 °C. Twenty minutes were allowed to equilibrate the temperature in the specimens at each temperature level. The epoxy specimen was cut into strips $50 \times 5 \times 1$ mm (L, w, h) from a cast epoxy sheet using a precision saw with a diamond blade. The specimen was placed in a three-point bending test configuration. One of the ends was glued with cyanoacrylate on its support to avoid any inadvertent shifts in the specimen over the duration of the test. A strain of 0.1% was prescribed in the center of the specimen by applying a central displacement Δ_0 of 0.4 mm while the load $P(t)$ response was measured. The temperature, load and displacement signal acquisition, control, and recording was accomplished using the Trios$^©$ software, which provides the relaxation modulus from a simple beam theory analysis, where the maximum stress and strain in the beam are given by $\sigma_{\max}(t) = (\frac{3}{2}\frac{L}{wh^2})P(t)$ and $\varepsilon_{\max}(t) = (\frac{6h}{L^2})\Delta(t)$. Given that a step in central displacement is applied,

$$E(t) = \left(\frac{L^3}{4wh^3}\right)\frac{P(t)}{\Delta_o}. \tag{15}$$

Figure 6 presents the master curve for the tensile relaxation modulus that was developed for 20 °C and RH55%. The Prony series fit to the measured tensile relaxation modulus compared favorably with the one that was obtained from the bulk and shear relaxation moduli. This can be more quantitatively assessed via the root-mean-square error in interconverted (E_i^C) and measured (E_i^M) tensile relaxation moduli, RSME $= \sqrt{\frac{\sum_{i=1}^{N}(E_i^C - E_i^M)^2}{N}}$ was used as a measure of the differences between the two sets of data. It was 0.065 MPa, or 0.3% of the rubbery tensile modulus, which suggests that the interconversion was successful.

The thermal shift factors that were used to obtain the master curves for bulk, shear, and tensile relaxation moduli are all shown in Fig. 7. The Arrhenius expression for the thermal shift factor,

$$\log_{10} a_T = \frac{\Delta F}{2.303R}\left(\frac{1}{T} - \frac{1}{T_R}\right), \tag{16}$$

was used below the glass transition, with an activation energy ΔF of 59.2 kcal per gram mole Kelvin and a reference temperature T_R of 293 K. Above the glass transition, the WLF
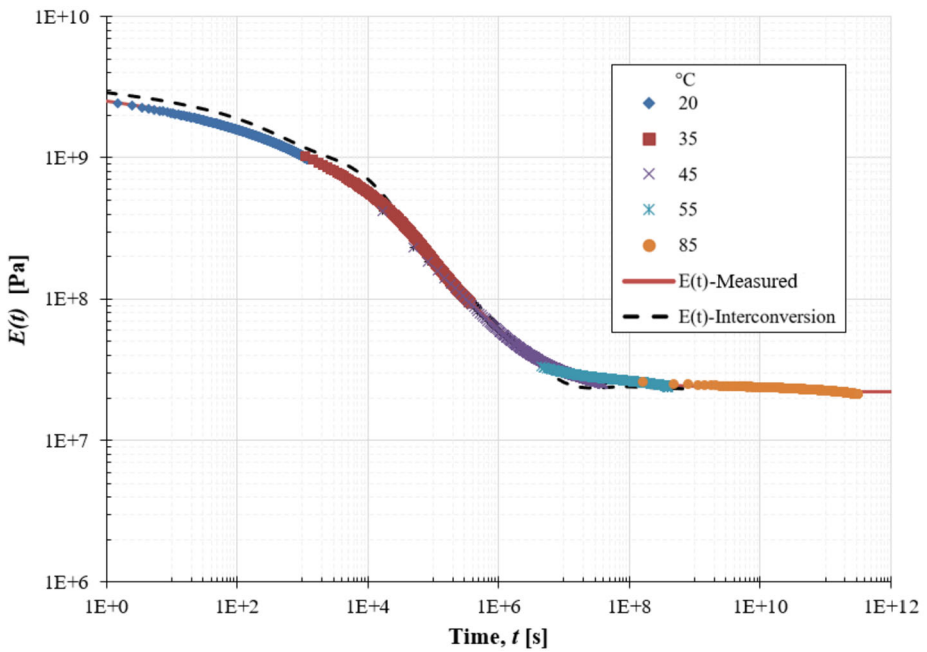
Fig. 6 Comparing master curves of the tensile relaxation modulus of the epoxy at 20 °C. Data from uniaxial tension relaxation experiments are compared with the results of interconversion

Fig. 7 Thermal shift factors for the tensile, bulk, and shear relaxation behavior of the epoxy
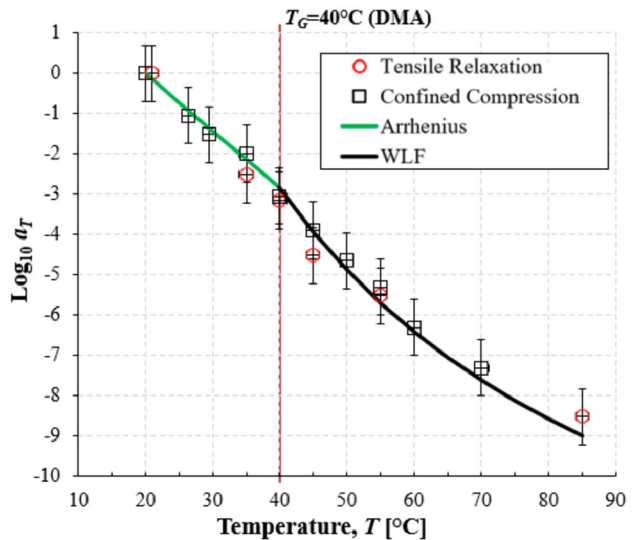
equation (Williams et al. 1955) for the thermal shift factor

$$\log_{10} a_T = \frac{-C_1(T - T_M)}{C_2 + T - T_M} \tag{17}$$

Fig. 8 A comparison of the measured shear stress-strain behavior with linearly viscoelastic predictions at four strain rates
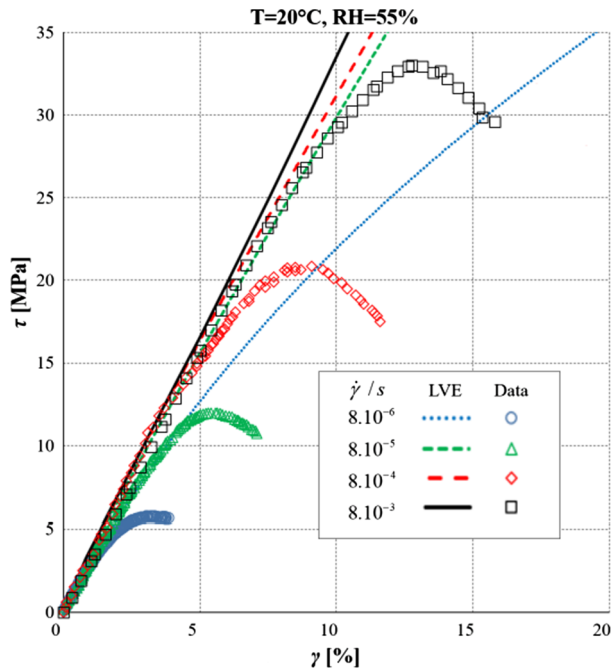
was adopted with constants $C_1 = 17.44$ and $C_2 = 51.6\text{K}$ for a reference temperature T_M that was 10 K below the glass transition. It can be seen that both expressions provided reasonable fits to the data from all three sets of relaxation data.

Limits of the linear behavior The limit of linearity under shear was established using the Arcan shear test (Popelar and Liechti 1997). The grips were made of steel to ensure adequate stiffness. The load was measured using a 9-kN load cell. The shear strain was determined based on the grip to grip measurement using two LVDTs (Sensotec) mounted in front and behind the specimen. All signals were acquired by a data acquisition board (model BNC-2090 National Instruments®) and recorded using a LabView© application developed for this test that acquired time, actuator displacement, LVDT displacement, and load data. The test was performed at room temperature (20 °C), a relative humidity of 55%, and four different applied displacement rates. The specimen was made from neat epoxy cast in a steel mold following the same cure procedures described previously.

The shear stress-strain relation under a strain rate $\dot{\gamma}_{12}$ is

$$\sigma_{12}(t) = \dot{\gamma}_{12} \int_0^t \mu\left(t' - \xi'\right) d\xi, \tag{18}$$

where $\dot{\gamma}_{12} = \dot{\Delta}/w$, Δ is the relative displacement of the grips, and w is the distance between them.

The results from the Arcan shear test are compared (Fig. 8) with the response obtained from Eq. (18) using the shear relaxation modulus for linear viscoelasticity. The measured responses followed the linearly viscoelastic prediction for relatively small strains. For the lowest strain rate, the limit of linear behavior was 0.5% strain. At the highest strain rate, the limit was 4%. Thus a large portion of the response was in the nonlinear range, thereby motivating the development of the nonlinearly viscoelastic model in the next section.

3 Nonlinear behavior

The results from the Arcan experiment and associated analysis demonstrated that linear viscoelasticity fails to predict the complete stress-strain response above certain strain limits. This section develops a nonlinear viscoelastic model based on the free-volume approach introduced by Knauss and Emri (1981, 1987) as modified by Popelar and Liechti (1997, 2003) to account for distortional effects. The model considers not only strain rate, history, and temperature effects but also thermal and hygral expansion as well as the individual contributions of dilatational and deviatoric strains, which actually introduce the nonlinearity.

Epoxy polymers are generally obtained from the reaction of polyepoxides with polyamines. Both parts, monomer and hardener, are mixed in the liquid state. During the curing period, crosslinking and solidification takes place in the form of a stiff and amorphous molecular structure. This structure is permanently secured by the presence of the newly formed crosslinks. Because of the stiffness and complexity of these crosslinked networks, the structure exists in a glassy state, like a supercooled liquid that cannot reconfigure itself into a purely crystalline state. Because of the locked-in amorphous molecular structure, there is a significant amount of specific volume that is taken up in the amorphous state relative to the same mass of polymer molecules in a crystalline arrangement. For any given temperature, this excess volume is called the free volume (Odegard and Bandyopadhyay 2011).

The presence of the free volume is due to the nonequilibrated amorphous state and has a significant impact on the density and the mechanical behavior of the polymer. Although the overall network is stiff, the free volume changes under mechanical and environmental conditions, which allows a degree of mobility of the polymer structure that affects the time scale of the material. Doolittle (1951) introduced the effect of free volume on a shift factor a that adjusts the real time scale to material clock or timescale based on the fractional free volume f of a specific state relative to the fractional free volume f_0 at some reference state, where B is a constant to be determined:

$$\log a = \frac{B}{2.303}\left(\frac{1}{f} - \frac{1}{f_0}\right). \tag{19}$$

Based on this result and the work of Knauss and Emri (1981, 1987), Popelar and Liechti (1997) suggested that deviatoric strains could contribute to the free volume in addition to the classically accepted components of volumetric thermal expansion, $\alpha_v \Delta T$, the volumetric hygral expansion due to change in solvent concentration, $\beta_v \Delta c$, and the mechanical dilatational strain $\delta\theta$, so that

$$\log a = -\frac{B_d}{2.303 f_d}\left(\frac{\alpha_v \Delta T + \beta_v \Delta c + \delta\theta}{f_d + \alpha_v \Delta T + \beta_v \Delta c + \delta\theta}\right) - \frac{B_s}{2.303 f_s}\left(\frac{\varepsilon_{eff}}{f_s + \varepsilon_{eff}}\right), \tag{20}$$

where $\varepsilon_{eff} = \sqrt{\frac{2}{3}e_{ij}e_{ij}}$ and $e_{ij}(t) = \varepsilon_{ij}(t) - \delta_{ij}\varepsilon_{kk}/3$. Ramp strain experiments that bring out the nonlinear response of the material in pure shear and uniaxial tension are used to determine the parameters (B_s, f_s) and (B_d, f_d, δ), respectively. The second term in Eq. (20) was the term that was added to account for nonlinear behavior in shear. The terms (f_s, f_d) represent reference values of free volume under shear and dilatation, respectively. The nonlinear behavior of the model comes from the dependence of the free volume on the mechanical dilatational and deviatoric strains (linear with no geometric nonlinearity) and their effect on
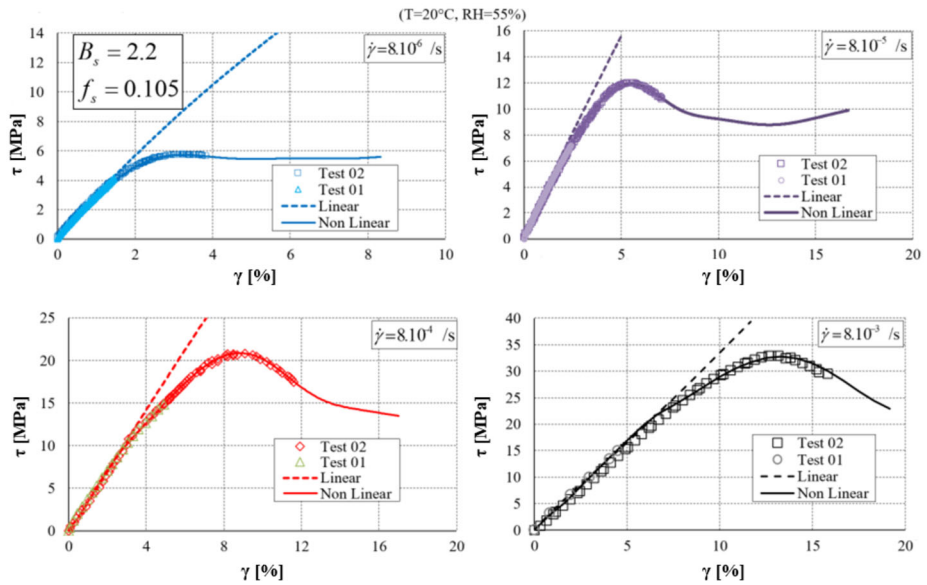
Fig. 9 Selecting $B_s = 2.2$ and $f_s = 0.105$ as the parameters for the shear response provided a suitably accurate model of the shear behavior in the nonlinearly viscoelastic regime

the reduced time through the shift factor so that the argument of the relaxation functions in Eqs. (5)–(6) becomes

$$t' - \xi' = \int_\xi^t \frac{d\xi}{a[T(\xi), c(\xi), \theta(\xi), \varepsilon_{eff}(\xi)]}. \tag{21}$$

Under these conditions, the integration of the constitutive equations is extremely convoluted, cannot be achieved analytically, and requires a numerical approach, which is outlined by Ferreira Vieira de Mattos (2017).

Evaluating the distortional parameters Consider a state of pure shear stress and strain under a constant temperature and moisture concentration. The dilatational part of the modified free volume shifting factor vanishes, as seen in Eq. (20). Therefore only two parameters B_s and f_s must be determined to calibrate the nonlinear viscoelastic model.

The Arcan shear test (Arcan et al. 1978) and particularly the version employed by Popelar and Liechti (1997) leads to a nearly uniform shear stress state in the gage section of the specimen, which satisfies the stress-strain state requirements to calibrate those parameters. All dimensions, measurements, and procedures were the same as previously described in Sect. 3. However, the reduced time is now only a function of the shear strain γ_{12} in Eq. (18), so that $\varepsilon_{eff}(\xi) = \sqrt{\frac{1}{3}\frac{\dot{\Delta}}{w}}\xi$.

Both distortional parameters were determined by considering the lowest shear strain rate and then checking at the selected values at other rates. The parameter f_s affects the location of the stress peak in the response to a ramp in strain. The results from four different experiments covering four decades in strain rate, all conducted at 20 °C and RH55 %, are shown in Fig. 9. As expected, the early stiffness changes with time due to the viscoelastic behavior of the epoxy before nonlinear effects begin to dominate as a maximum stress is

achieved. In the model the ensuing drop in stress reached a minimum followed by stiffening, which was provided by a strain-dependent rubbery shear modulus to $\mu_\infty = \tilde{\mu}_\infty \exp(\varepsilon_{eff}/\varepsilon_0)$, where $\tilde{\mu}_\infty$ and ε_0 are fitting parameters (Popelar and Liechti 2003). This avoids the unlimited softening, which results from the manner in which the nonlinear behavior is introduced by the shift factor in Eq. (20). Unfortunately, the specimens all broke before any minimum was detected. The best fit to the response at the lowest rate was provided by $B_s = 2.2$ and $f_s = 0.105$, which also turned out to deliver good agreement with the measured responses at all the other strain rates. The stiffening behavior was established by selecting ε_0 as 0.04. The parameter $\tilde{\mu}_\infty$ was taken to be the rubbery modulus that was determined for the linearly viscoelastic response.

Evaluating the dilatational parameters　Determining the distortional parameters B_s and f_s is simpler than determining the dilatational ones, B_d, f_d, and δ, mainly because hygrothermal effects also have to be considered. Although confined compression data could be used for this exercise, uniaxial tension has proven (Chevellard et al. 2012) to be more discriminating, even though it contains both dilatational and distortional effects. The diffusion and thermal behavior of the epoxy are considered first.

Water absorption　The water absorption test was used to determine the amount of water absorbed under a range of relative humidity conditions. A weight gain measurement based on ASTM D570 was followed. The specimens were made from neat epoxy, cast in 50.8-mm-diameter disks that were 6.35-mm thick. The specimens were dried in a vacuum chamber and weighed with an electrical precision scale with a resolution of 0.01 mg until equilibrium was achieved. The equilibrated weight was taken as the reference value W_0. After this conditioning time, the specimens were immersed in deionized water. Specimens were periodically removed from the environment; their surfaces were patted dry with lint-free cleaning paper and weighed. The weight and conditioning time were recorded to calculate the moisture content. The specimen was then reimmersed in the deionized water, and the whole procedure was repeated until saturation was achieved. The moisture loss in the specimen during surface drying and weighing was neglected since each measurement step took less than 5 minutes. The water absorption was expressed as the percentage $(\Delta W / W_0)$ increase in weight over the reference value. All the tests were conducted under room temperature that was approximately constant at 21 ± 1 °C. The moisture content was plotted as the weight gain versus the square root of the conditioning time. Fujita (1961) has compared non-Fickian and Fickian diffusion processes and made the following observations:

(a) For both absorption and desorption, plots of $\Delta W / W_0$ against $t^{1/2}$ are initially linear, and this linearity should extend to at least 0.6% for absorption;
(b) Beyond the linear region, the response is concave against the abscissa;
(c) Plots of $\Delta W / W_0$ against $t^{1/2}/h$, which are termed reduced absorption curves, should coincide for different specimen thickness h;
(d) Plots of $\Delta W / W_0$ against $t^{1/2}/h$ for absorption and desorption will only coincide when the diffusion coefficient D does not vary with the concentration of the sorbent.

As observed in Fig. 10, the bulk epoxy exhibited classical Fickian diffusion behavior as characterized by an initial linear increase in weight, followed by a plateau corresponding to the saturation moisture content W_∞. The maximum moisture content that was attained was 1.31%, which agrees with the value 1.3 ± 0.1% found by Canal and Michaud (2014).

The results provided the diffusion coefficient D from the solution

$$W(t) = W_0 + (W_\infty - W_0)\frac{4}{h}\sqrt{\frac{Dt}{\pi}} \tag{22}$$

$$t_m^{1/2} = (1530 \pm 80)\,\text{s}^{1/2}$$
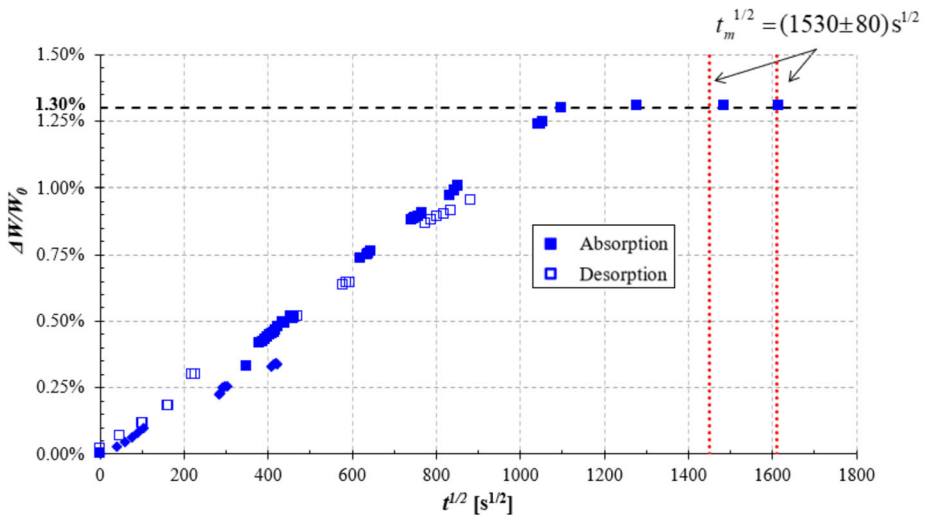
Fig. 10 Moisture content as a function of square root of time at a temperature of 21 °C

to Fick's second law. The diffusion coefficient was $1.17 \pm 0.12 \times 10^{-11}$ m^2/s. This value was used in the evaluation of the hygral expansion coefficient presented in the following section. The time t_m required to attain 99.9% of the maximum moisture content was $2.33 \pm 0.24 \times 10^6$ s.

Hygral expansion   Perhaps the simplest way to estimate the coefficient of hygral expansion is using the weight gain measurements to compute the volume change based on the assumption that the density remains constant. However, more direct measurements do not require any such assumptions and are preferable. In the past, essentially pointwise measurements have been made (Park et al. 2004), but full field methods provide more data and may also be more discriminating between Fickian and more general forms of diffusion.

Accordingly, an experiment was designed to measure the out-of-plane displacements in an epoxy disk to radial diffusion of the humid environment in a previously dried epoxy specimen. The measurements allowed the hygral expansion coefficient β_v to be determined directly at many radial locations. The top surface of the specimen was coated in order to direct diffusion from the edge to the center of the disk.

This experiment employs a Michelson interferometer (Fig. 11a), which is a common configuration for optical interferometry. The light from a coherent light source is split into two beams using a beam splitter. Each one is reflected toward the beam splitter, which then combines their amplitudes interferometrically. One of the reflection surfaces is a mirror that can be tilted using two knobs. The other surface of reflection is the top surface of the specimen.

The relative humidity and the temperature were measured using a probe (PCMINI52-3-SX-H-X-CB-F03) and recorded by a LabView© application, which acquired these data every 10 seconds. The fringe pattern was recorded using a camera that captured images each minute for the first hour and then every five minutes until the experiment was complete at 24 hours. It was necessary to run the experiment using two computers, one for the automated image recording and the other to acquire the environmental data through a LabView application. The computers were clocked by the network to record all data using the same
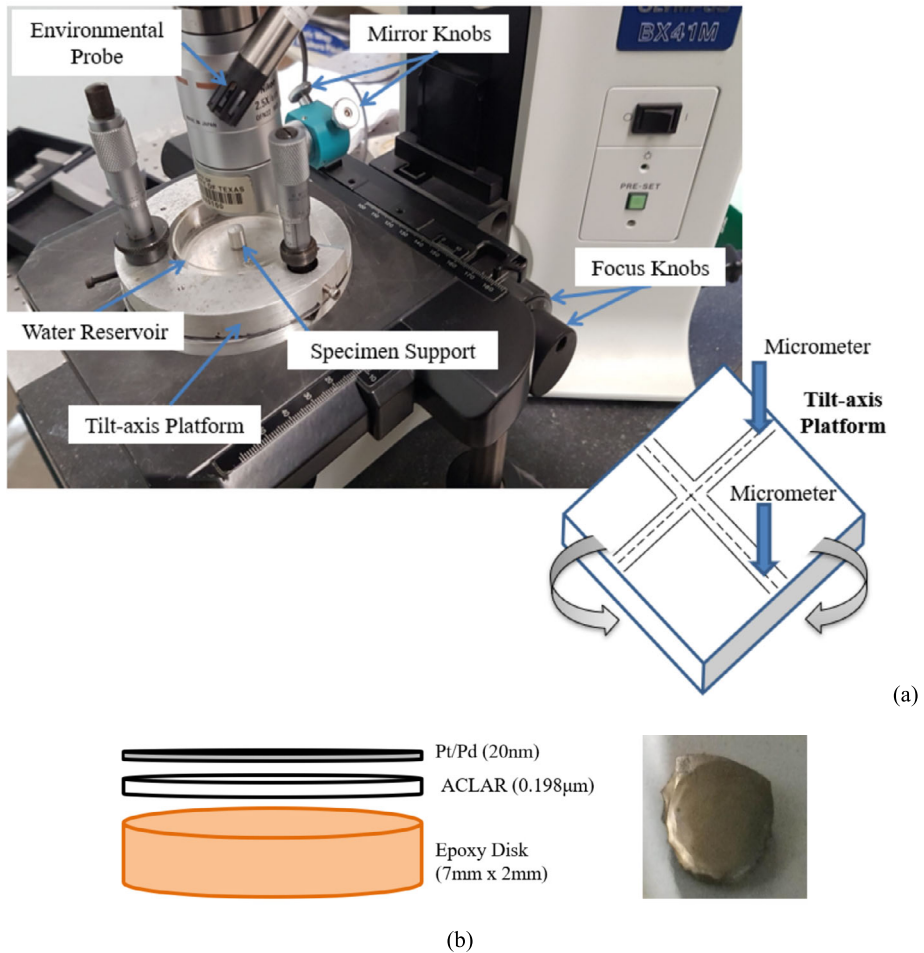
Fig. 11 (a) Apparatus for the hygral expansion test; (b) Geometry and top view of the specimen

reference time. The sample was weighed using a 0.01-mg precision scale at the beginning of the test after being dried out under vacuum and at the end as a global measurement of the weight gain. The specimen was placed on the top of a support to be kept above the water level. A kinematic tilt-axis platform was used to bring the specimen surface into close alignment with the interferometer. Fine tuning was achieved by adjusting the two knobs on the interferometer (Fig. 11b).

The specimen was required to present a sufficiently flat and smooth surface to the interferometer and at the same time be reflective enough to allow fringes to form. In addition, the desire for moisture to diffuse radially into the specimen required a sealant to be applied to the top surface of the specimen. A 0.19-μm-thick film of ACLAR® turned out to be a suitable choice.

ACLAR is a poly-chloro-tri-fluoro-ethylene (PCTFE) film. Masurovsky and Bunge (1968) were the first to describe and clearly demonstrate the useful chemical and physical properties of ACLAR for both tissue culture and electron microscopy. From the beginning

it was used in the space program, and its properties were found to be helpful for biomedical research and applications. ACLAR is crystal clear, biochemically inert, chemical resistant, plasticizer and stabilizer free, can be processed over the same range as other thermoformable films, transparent to UV, nonflammable, and nonageing, has a low dielectric constant and dissipation, is high in dielectric strength, can be sterilized, and is unsurpassed as a moisture barrier and very compliant. These last two characteristics were particularly compelling in the selection of ACLAR as a sealant for this experiment. Although the ACLAR provided a suitably flat surface, its reflectivity was insufficient to provide visible fringes. This issue was resolved by coating the ACLAR surface with a 20-nm Pt/Pd layer.

The epoxy was prepared following the recipe for all neat epoxy specimens already presented. After pouring the epoxy into the mold, a piece of ACLAR was placed over the top. The surface was flattened by placing a smooth and flat weight on top of the ACLAR while the epoxy cured at 100 °C for two hours. Figure 11b presents the final geometric configuration, including dimensions and the top view of the specimen.

An environmental chamber was formed around the specimen using a compliant polymer film. As a calibration of the system, the temperature and the relative humidity were recorded for a 24-hour period once the chamber had been closed and the water reservoir had been filled. Once the chamber was closed, the relative humidity rose to an equilibrium value of 84 ± 2.5 RH% in less than 30 minutes. During this time, the temperature in the chamber was 20.7 ± 1 °C. The performance of the chamber was monitored in the same way during experiments with the specimen in the chamber, and similar performance was noted.

A typical fringe pattern is shown in Fig. 12. For fringe analysis, each image was converted to a gray scale and normalized by a MATLAB© application. The intensity value of each pixel was stored in a matrix. A radial intensity profile was selected from this matrix for further analysis. The intensity peaks correspond to bright fringes, which were numbered, and their locations recorded using a semiautomatic system. The peak detection procedure makes use of the fact that the first derivative of a peak has a downward-going zero-crossing at the peak maximum. However, the presence of any noise can lead to many false zero-crossings. To avoid this problem, the present technique first smooths the first derivative of the intensity profile before seeking downward-going zero-crossings. Only the peaks with slope exceeding a "slope threshold" were selected. By carefully adjusting the smoothing window, slope threshold, and amplitude threshold it was possible to detect only the desired peaks and ignore peaks that are too small, too wide, or too narrow. Moreover, this technique was extended to estimate the position, height, and width of each peak by least-square fitting of a segment of the original unsmoothed signal in the vicinity of the zero-crossing. Thus, even if heavy smoothing of the first derivative was necessary to provide reliable discrimination against noise peaks, the peak parameters extracted by curve fitting are not distorted by the smoothing, and the effect of random noise in the signal is reduced by curve fitting over multiple data points in the peak.

The out-of-plane displacement profiles were determined with a resolution of 275 nm ($\lambda/2$). The results from an experiment are shown as a function of time in Fig. 12b, where they are compared with the analysis given in detail by Ferreira Vieira de Mattos (2017) and are summarized here.

The radial distribution of the solvent concentration C as a function of time t is given by

$$\frac{C}{C_0} = 1 - \frac{2}{a} \sum_{n=1}^{\infty} \frac{1}{\alpha_n} \frac{J_0(\alpha_n r)}{J_1(\alpha_n a)} e^{-D\alpha_n^2 t}, \qquad (23)$$

where C_0 is the solvent concentration at $r = a$, the edge of the specimen. The functions J_0 and J_1 are the zero- and first-order Bessel functions, and α_n are the roots of $J_0(\alpha_n a) = 0$.
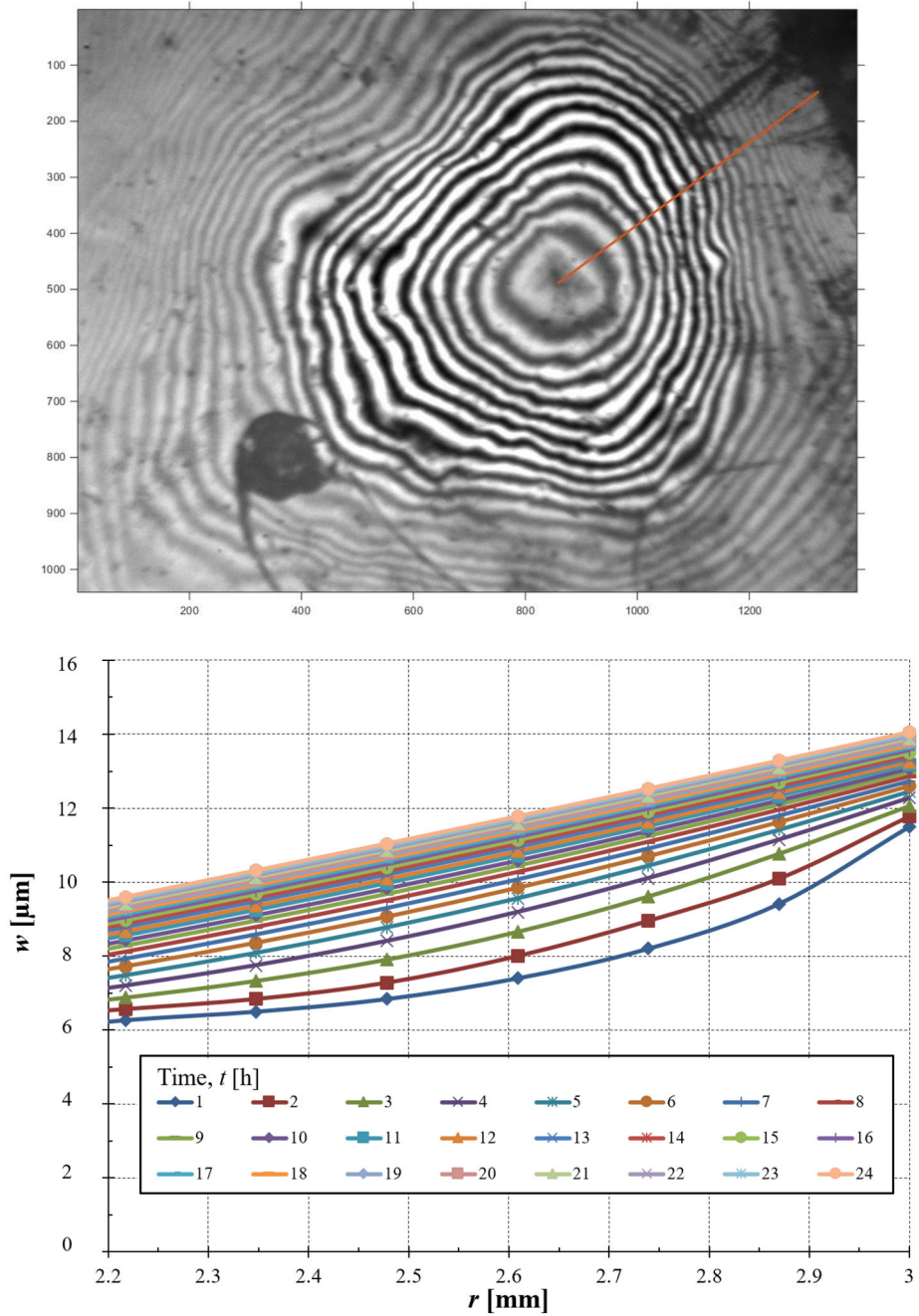
Fig. 12 Out-of-plane displacements of the outer surface of an epoxy disk during the radial diffusion of moisture: (**a**) a typical fringe pattern and (**b**) a comparison of displacement profiles

The out-of-plane displacement is given by

$$
w = \frac{vh}{v-1}\left\{ 2A + \frac{(1+v)}{2C_0}\left\{ 2 - r + \frac{2}{a}\sum_{n=1}^{\infty} \frac{e^{-\alpha_n^2 Dt}}{\alpha_n J_1(\alpha_n a)}\left[\left(1 - \frac{1}{\alpha_n^2}\right)J_2(\alpha_n r)\right.\right.\right.
$$

$$
\left.\left.\left. - 2J_0(\alpha_n r)\right]\right\}\beta_v\right\} - \frac{v+1}{v-1}\beta_v C, \tag{24}
$$

where

$$
A = \frac{(1+v)}{2C_0}\left\{ a - 2 + \frac{2}{a}\sum_{n=1}^{\infty} \frac{1}{\alpha_n J_1(\alpha_n a)}\left[2J_0(\alpha_n a) + J_2(\alpha_n a)\left(\frac{1}{\alpha_n^2} - 1\right)\right]\right\}\beta_v
$$

$$
+ C(a)\beta_v, \tag{25}
$$

and h is the thickness of the epoxy disk with Poisson's ratio v. The epoxy was taken to be in its glassy state for the duration of the experiment. By Eq. (24) the measured displacement field and the diffusivity were used to determine the hygral expansion coefficient at 0.435 ± 0.017. A series of least square fits at various radial locations was used to determine the value of β_v that minimizes the error ($R^2 = 0.9252$). A first approximation of the hygral expansion coefficient using the weight gain evaluated $\beta_v \sim 0.381$, a value that represents a 12.4% error compared that found using interferometry.

The high degree of correlation in determining β_v on the basis of Fickian diffusion indicates that non-Fickian effects were not present in this experiment. This is further confirmed by the smooth out-of-plane displacements that were measured (Fig. 12b) and the lack of any diffusion fronts.

Thermal expansion The coefficient of thermal expansion was determined using a DMA (RSA G2). The specimen had the same dimensions as the one used in the three-point bending relaxation test. However, in this case the specimen was placed in the uniaxial tension configuration of the instrument. Ideally, the expansion of the specimen as the temperature is increased should be measured under zero load. Due to the manner in which the instrument control is configured, load control with a constant load of 1.9 N (0.38 MPa) was applied while the temperature was increased and the change in length of the specimen was measured. The change in length with temperature then provides the coefficients of thermal expansion above and below the glass transition. Because the displacement measurement includes any expansion of the driveshaft and clamps, a calibration of the instrument with a known standard was required. Subtracting out these spurious contributions to the measured displacement then provided the thermal response of the specimen itself.

The calibration was conducted on an aluminum sample with the same dimensions as the epoxy specimen. The specimen was mounted in the tension clamps of the DMA. Data were collected from 25 °C to 78 °C. The temperature in the chamber was increased at 1 °C/minute to guarantee that the temperature in the specimen was uniform. The coefficient of thermal expansion adopted for the aluminum was 2.5×10^{-5} K^{-1}.

The expansion of the epoxy was initially linear (Fig. 13), but as the temperature increased and the material reached the glass transition, the expansion became nonlinear due to conformational changes in the epoxy. Beyond the transition region, the expansion became linear again. Both linear portions of the data were fitted by a linear regression. The corresponding coefficients of thermal expansion were 1.93×10^{-4} /°C, $T < T_g$ and 3.20×10^{-4} /°C, $T \geq T_g$.
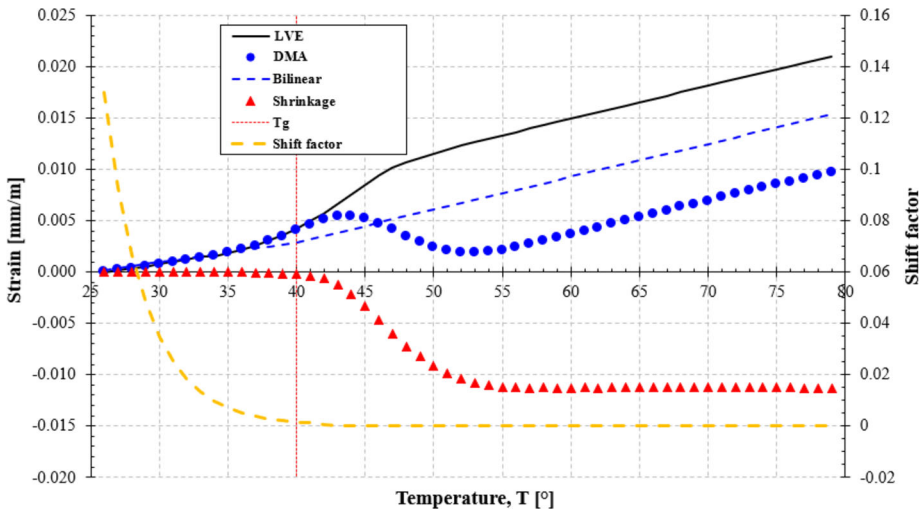
Fig. 13 Comparison of the measured thermal expansion with the results of a linearly viscoelastic analysis. The bilinear form and the shift factor are shown for guidance. The shrinkage was obtained by subtracting the measured response from the results of the analysis

As a consistency check, the experiment was modeled using the measured coefficients of thermal expansion and the measured linearly viscoelastic behavior, including the temperature shift factor behavior above and below the glass transition (Fig. 7). The result is compared with the measured response (Fig. 13), and the bilinear thermal expansion behavior is added as a guide.

For temperatures below the glass transition, the viscoelastic model predicted the measured strain response reasonably well. In the very beginning the expansion is dominated by the thermal expansion over and above the effect of the small preload, which accounts for the approximately linear response. However, as the free volume increases, the shift factor drops (Fig. 13), thereby accelerating the material clock until the rubbery state is reached. Between T_g and 53 °C the measured strain follows the model until it reaches a peak value and starts to decay. This effect was attributed to physical aging that promotes shrinkage in the material. The shrinkage shown in the graph was extracted from the measurements and the predictions from the linearly viscoelastic analysis. It eventually becomes constant, and a linear thermal response returns where the prominent effect again is thermal expansion.

Uniaxial tension   Uniaxial tension has both distortional and dilatational components, which in turn contribute to the shift factor and associated changes in the material clock when the strains are large enough. Since the distortional behavior and contributions from the hygrothermal expansion are known, the stage is set to determine the dilatational parameters. An iterative process was implemented to determine the dilatational parameters at the highest humidity (and related temperature) and lowest strain rate. The selected parameter set for dilatation was then validated at other temperatures, strain rates, and moisture conditions.

The specimen, its dimensions, and schematic of the test and strain gages are shown in Fig. 14. The specimen gage length, width, and thickness (127, 12.7, and 2.54 mm, respectively) were chosen to allow a pair of microscoping extensometers from Psylotech® to be mounted on it.
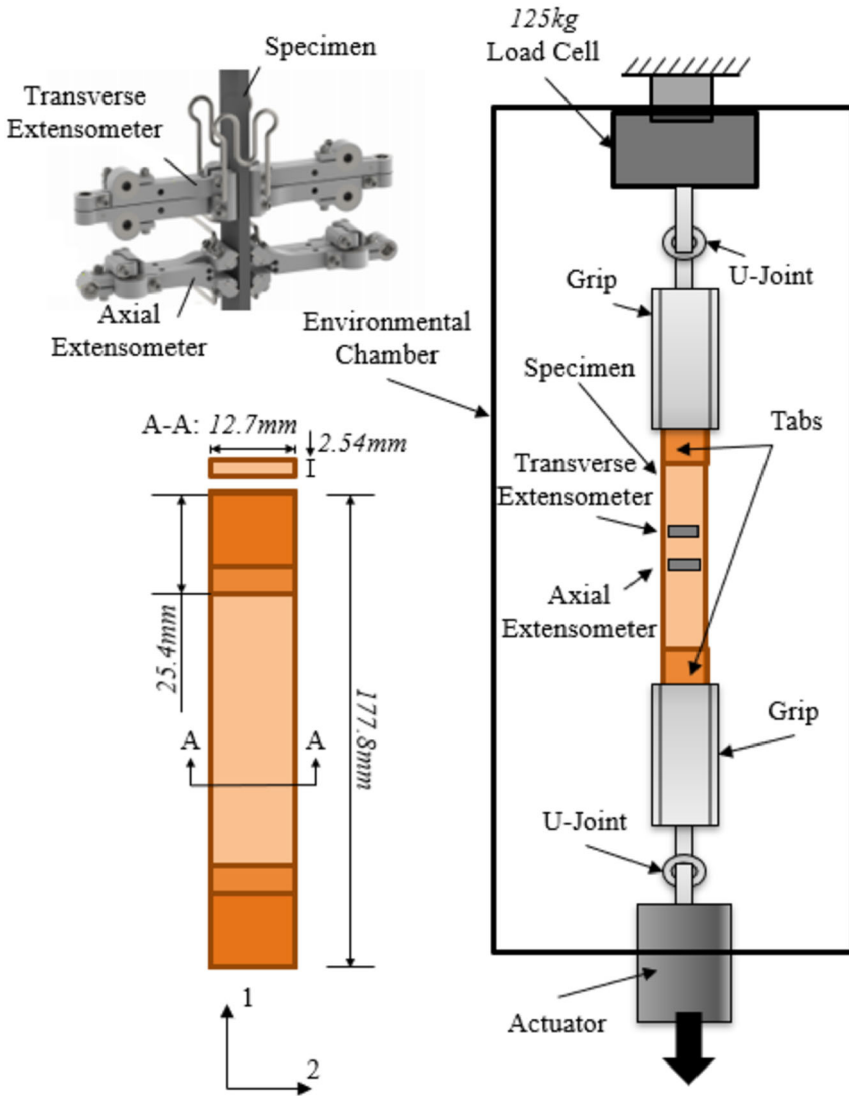
Fig. 14 Uniaxial tensile test specimen and schematic of test

Another constraint was minimizing the saturation time, which was estimated using Fickian diffusion and checked with a scale with a resolution of 0.01 mg. Tabs were added to both ends to minimize stress concentrations near the grips as well as damage or slip. A pair of grips was designed to fit the specimens and allow a U-Joint to be inserted between the grips and the servohydraulic machine cross-head and actuator. A 1.2-kN load cell (Omega LCM402-250) was inserted in the load train inside an environmental chamber, which was able to prescribe and control the temperature and moisture levels to within 1 °C and 2%RH, respectively. A LabView application was developed to acquire the actuator displacement from the servohydraulic machine (MTS), axial and transverse strain, and load. All specimens eventually failed in the gage section.
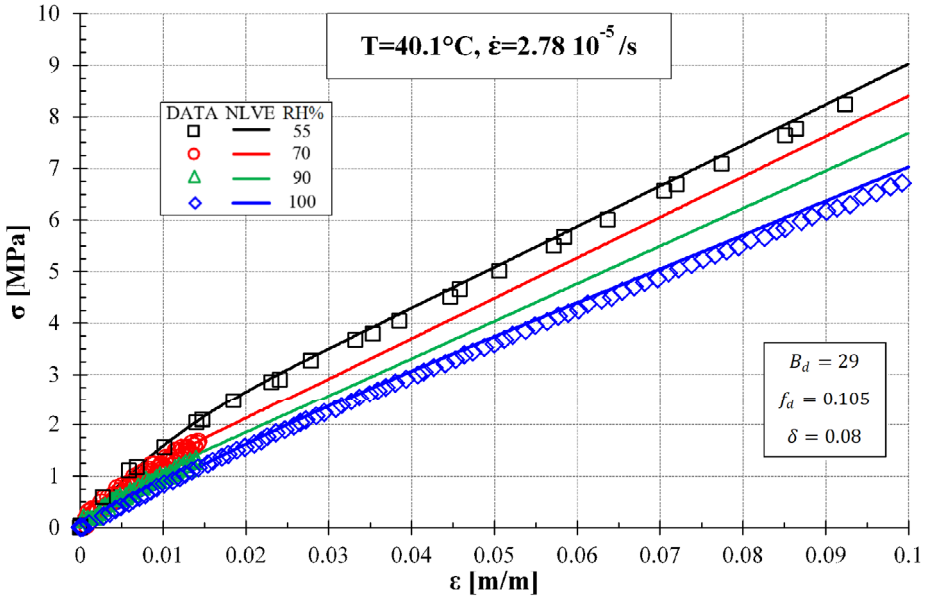
Fig. 15 Comparing the results from uniaxial tensile tests at several humidity levels with predictions made with the converged values of the dilatational parameters

Under a ramp in strain $\varepsilon_{11}(t) = \dot{\varepsilon}_{11}t$, the axial stress is

$$\sigma_{11}(t) = \int_0^t E(t' - \xi') \frac{\partial \varepsilon_{11}(\xi)}{\partial \xi} \, d\xi. \tag{26}$$

The transverse strain can be found by using Poisson's ratio in relaxation

$$\varepsilon_{22}(t) = \varepsilon_{33}(t) = \int_0^t v_r(t' - \xi') \frac{\partial \varepsilon_{11}(\xi)}{\partial \xi} \, d\xi. \tag{27}$$

The dilatational $\theta(t)$ and the effective distortional strain $\varepsilon_{eff}(t)$ are, respectively, $\theta(t) = \varepsilon_{11}(t) + 2\varepsilon_{22}(t)$ and $\varepsilon_{eff}(t) = \sqrt{\frac{2}{3}e_{ij}e_{ij}} = \sqrt{\frac{2}{3}(e_{11}^2 + 2e_{22}^2)} = \frac{2}{3}(\varepsilon_{11}(t) - \varepsilon_{22}(t))$. These were used in Eq. (26) to determine the reduced time in the argument of the tensile relaxation modulus as the dilatational parameters were iterated on in comparing the resulting responses against the measured one. Figure 15 presents the results for the same temperature and rate, but for different moisture levels. Some specimens failed in the gage section at strains less than 2%. The results are plotted from the specimens that reached the highest strain level for each case. The nonlinear viscoelastic model predictions are plotted as solid lines. The converged values of the dilatational parameters are $B_d = 29$, $f_d = 0.105$, and $\delta = 0.08$.

The effect of temperature under uniaxial tension at a strain rate of 1.67×10^{-3} /s with relative humidity of 55% is shown in Fig. 16. All the specimens failed in the gage section, and the linearly viscoelastic predictions are presented in dashed lines for comparison. The nonlinear viscoelastic predictions (solid lines) are in excellent agreement with the measured responses (markers). The nonlinear effects appear sooner at higher temperatures, and the model was able to capture the initial portion of the observed softening behavior at the lowest temperature.
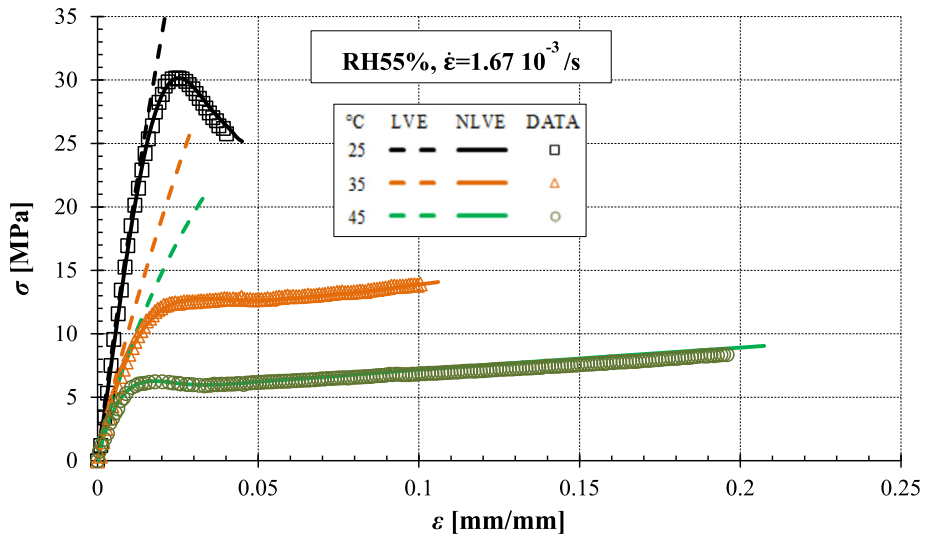
Fig. 16 Comparing the results from uniaxial tensile tests at several temperature levels with predictions made with the converged values of the dilatational parameters

At this point, it is instructive to catalog the parameters that have been extracted on the basis of the modified free-volume theory for four different polymers in six references (Table 2). The polymers are a urethane adhesive (Ashland), epoxy 1 (Araldite GY 505 and HY 955), epoxy 2 (Araldite GY 505 and Aradur 955-2), and a polyurea coating (Isonate 143L and Versalink P1000). In the original work by Popelar and Liechti (1997), there were no measurements of the coefficient of thermal expansion, which allowed the dilatational parameter δ for epoxy 1 to be arbitrarily selected at a value of 1. This led to the values of the dilatational parameters for epoxy 1 to be considerably smaller than the values obtained in subsequent studies (Arzoumanidis and Liechti 2003; Park et al. 2004), whose distortional and dilatational parameters values for the epoxy are all very consistent. Epoxy 2, the material considered in this study, had the same resin, but the hardener had been changed. Nonetheless, we can see that the extracted distortional and dilatational parameters remained the same. The values of the parameters for the polyurea are quite different, but it should be borne in mind that it is an elastomeric material. The urethane adhesive has a glass transition temperature of approximately 60 °C, and the values of its parameters were closer to those of the epoxy.

4 Conclusions

Experiments were designed and performed to characterize the linear and nonlinear viscoelastic behavior of an epoxy adhesive. Two functions are required to characterize a homogeneous, isotropic, and linearly viscoelastic material. A confined compression experiment was performed following the standard protocol established by Tschoegl et al. (2002), which requires that the basic viscoelastic functions be determined simultaneously on the same specimen, under the same environmental conditions. The shear and bulk relaxation moduli of the epoxy were determined and fit to Prony series. The tensile relaxation modulus and

Table 2 Summary of distortional and dilatational parameters obtained for urethane and epoxy adhesives and a polyurea coating

Reference	Polymer	B_s	f_s	B_d	f_d	δ
Popelar and Liechti (1997, 2003)	Urethane	0.4606	0.1	0.2303	0.1	1
Popelar and Liechti (1997, 2003)	Epoxy 1	3.25	0.1	0.5	0.1	1
Arzoumanidis and Liechti (2003)	Epoxy 1	2.2	0.105	29	0.1	0.08
Park et al. (2004)	Epoxy 1	2.2	0.105	29	0.1	0.08
Chevellard et al. (2012)	Polyurea	4.0	0.245	0.2	0.016	−0.8
Ferreira Vieira de Mattos (2017)	Epoxy 2	2.2	0.105	29	0.105	0.08

Poisson's ratio in relaxation were deduced using an interconversion procedure, and the resulting data were also fit with Prony series. A separate tensile relaxation test was conducted, and the measured and deduced tensile relaxations were in good agreement. The glass transition temperature was determined to be 40 °C using the tan δ approach. The shift factors that were used for all the experiments were fitted to Arrhenius and WLF equations below and above the glass transition, respectively. The viscoelastic functions were then used to establish the limits of linear viscoelasticity using the Arcan shear test. The results from the Arcan experiment and associated analysis demonstrated that linear viscoelasticity fails to predict the complete stress-strain response above certain strain limits. For the lowest strain rate, the limit of linear response was 0.5% strain. This limit corresponds to a relatively small portion of the complete stress-strain response, thereby motivating nonlinear characterization at different strain rates, temperatures, and moisture levels.

A nonlinear viscoelastic model based on free-volume approach modified by Popelar and Liechti (1997, 2003) was adopted. The model considers the effects of thermal and hygral expansion as well as the individual contributions of the dilatational and deviatoric strains, which introduce nonlinearity. The distortional parameters were evaluated from the Arcan shear tests considering the lowest shear strain rate at 20 °C and a relative humidity of 55%. The nonlinear viscoelastic model was used to predict the stress-strain response at the other shear strain rates and provided good agreement without any adjustment of parameters. The dilatational parameters were extracted from uniaxial tensile tests. To predict the nonlinear viscoelastic behavior for different temperatures and moisture conditions, the coefficient of thermal and hygral expansion were also determined. The diffusion coefficient was also measured from experiments that established that the epoxy follows Fickian diffusion. The uniaxial stress-strain behavior for different environmental conditions was successfully predicted. Therefore the nonlinearly viscoelastic model based on the modified free volume approach can accurately predict the stress-strain response based on the applied strain history, the thermal and hygral expansions, and include the nonlinearities introduced by the mechanical dilatational and distortional strain.

Publisher's Note   Springer Nature remains neutral with regard to jurisdictional claims in published maps and institutional affiliations.

Appendix

The confined compression tests for the bulk and shear relaxation moduli were conducted at 20 °C, 26.4 °C, 29.5 °C, 35 °C, 40 °C, 45 °C, 50 °C, 55 °C, 60 °C, and 70 °C. The relaxation data at each temperature are shown in Fig. 17.

(a)

(b)
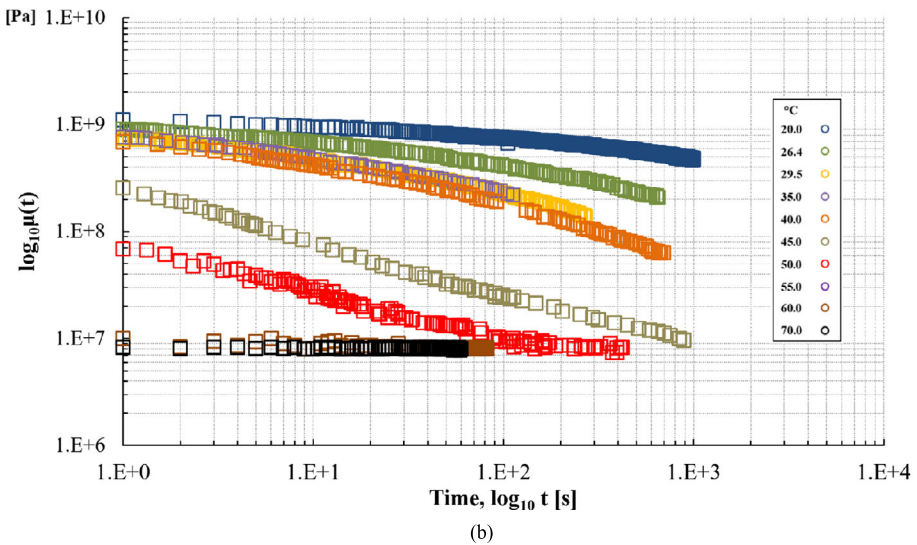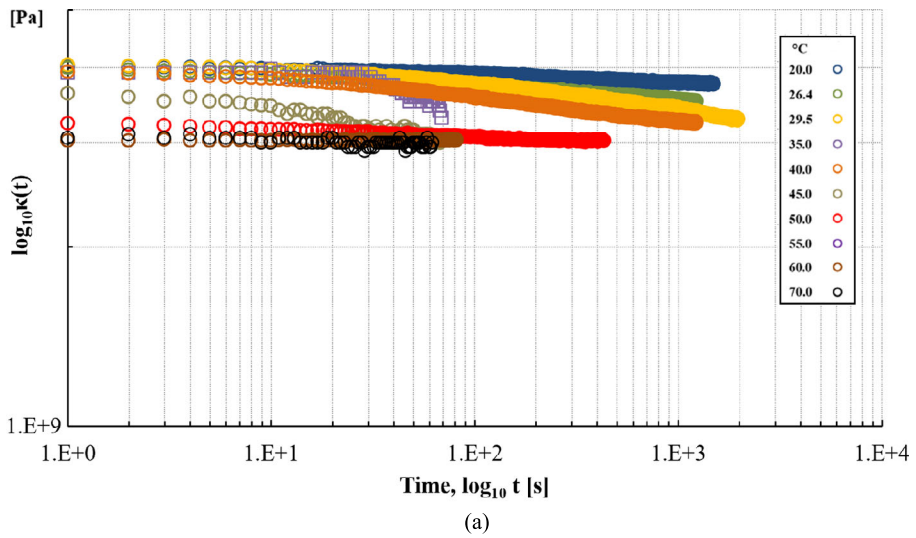
Fig. 17 Data obtained from confined compression tests prior to time–temperature shifting: (**a**) bulk and (**b**) shear relaxation moduli

References

Adolf, D.B., Chambers, R.S., Caruthers, J.M.: Extensive validation of a thermodynamically consistent, nonlinear viscoelastic model for glassy polymers. Polymer **45**, 4599–4621 (2004)

Arcan, M., Hashin, Z., Voloshin, A.: A method to produce uniform plane stress states with applications to fiber-reinforced materials. Exp. Mech. **18**(2), 141–146 (1978)

Arzoumanidis, G.A., Liechti, K.M.: Linear viscoelastic property measurement and its significance to some nonlinear viscoelasticity models. Mech. Time-Depend. Mater. **7**, 209–250 (2003)

Bradshaw, R.D., Brinson, L.C.: A sign control method for fitting and interconverting material functions for linearly viscoelastic solids. Mech. Time-Depend. Mater. **1**(1), 85–108 (1997)

Canal, L.P., Michaud, V.: Micro-scale modeling of water diffusion in adhesive composite joints. Compos. Struct. **111**, 340–348 (2014)

Caruthers, J.M., Adolf, D.B., Chambers, R.S., Shrikhande, P.: A thermodynamically consistent, nonlinear viscoelastic approach for modeling glassy polymers. Polymer **45**, 4577–4597 (2004)

Chevellard, G., Ravi-Chandar, K., Liechti, K.: Modeling the nonlinear viscoelastic behavior of polyurea using a distortion modified free volume approach. Mech. Time-Depend. Mater. **16**(2), 181–203 (2012). https://doi.org/10.1007/s11043-011-9146-9

Cost, T.L., Becker, E.B.: A multidata method of approximate Laplace transform inversion. Int. J. Numer. Methods Eng. **2**(2), 207–219 (1970)

Doolittle, A.K.: Studies in Newtonian flow II: the dependence of the viscosity of liquids on free-space. J. Appl. Mech. **22**, 1471–1475 (1951)

Drozdov, A.D.: Accretion of ageing, viscoelastic bodies under conditions of volume solidification. Mech. Solids **23**, 98–103 (1988)

Emri, I., Tschoegl, N.: Generating line spectra from experimental responses. Part I: relaxation modulus and creep compliance. Rheol. Acta **32**(3), 311–322 (1993)

Ferreira Vieira de Mattos, D.: Effect of moisture on mixed-mode traction-separation relations of a glass/epoxy interface. PhD Dissertation, University of Texas Austin (2017)

Fillers, R.W., Tschoegl, N.W.: The effect of pressure on the mechanical properties of polymers. Trans. Soc. Rheol. **21**, 51–100 (1977)

Fujita, H.: Diffusion in polymer-diluent systems. In: Fortschritte Der Hochpolymeren-Forschung, pp. 1–47. Springer, Berlin (1961)

Guth, E., Wack, P.E., Anthony, R.L.: Significance of the equation for state for rubber. J. Appl. Phys. **17**, 347–351 (1946)

Knauss, W.G., Emri, I.: Non-linear viscoelasticity based on free volume consideration. Comput. Struct. **13**, 123–128 (1981)

Knauss, W.G., Emri, I.: Volume change and the nonlinearly thermo-viscoelastic constitution of polymers. Polym. Eng. Sci. **27**(21), 86–100 (1987)

Knauss, W.G., Kenner, V.H.: On the hygrothermomechanical characterization of polyvinyl acetate. J. Appl. Phys. **51**(10), 5131–5136 (1980)

Leaderman, H.: Elastic and Creep Properties of Filamentous Materials and Other High Polymers. The Textile Foundation, Washington (1943)

Losi, G.U., Knauss, W.G.: Free volume theory and nonlinear thermoviscoelasticity. Polym. Eng. Sci. **32**(8), 542–557 (1992)

Lustig, S.R., Shay, R.M. Jr, Caruthers, J.M.: Thermodynamic constitutive equations for materials with memory on a material time scale. J. Rheol. **40**(1), 69–106 (1996)

Ma, Z., Ravi-Chandar, K.: Confined compression: a stable homogeneous deformation for constitutive characterization. Exp. Mech. **40**, 38–45 (2000)

Makhmutov, I., Sorina, T., Suvorova, Y.V., Surgucheva, A.: Failure of composites taking into account the effects of temperature and moisture. Mech. Compos. Mater. **19**(2), 175–180 (1983)

Masurovsky, E.B., Bunge, R.P.: Fluoroplastic coverslips for long-term nerve tissue culture. Stain Technol. **43**(3), 161–165 (1968)

Medvedev, G.A., Caruthers, J.M.: A comparison of constitutive descriptions of the thermo-mechanical behavior of polymeric glasses. In: Roth, C.B. (ed.) Polymer Glasses. Taylor and Francis, London (2017)

Odegard, G., Bandyopadhyay, A.: Physical aging of epoxy polymers and their composites. J. Polym. Sci., Part B, Polym. Phys. **49**(24), 1695–1716 (2011)

Park, S.J., Liechti, K.M., Roy, S.: Simplified bulk experiments and hygrothermal nonlinear viscoelasticity. Mech. Time-Depend. Mater. **8**, 303–344 (2004)

Popelar, C.F., Liechti, K.M.: Multiaxial nonlinear viscoelastic characterization and modeling of a structural adhesive. J. Eng. Mater. Technol. **119**, 205–210 (1997)

Popelar, C.F., Liechti, K.M.: A distortion-modified free volume theory for nonlinear viscoelastic behavior. Mech. Time-Depend. Mater. **7**(2), 89–141 (2003)

Schapery, R.A.: A simple collocation method for fitting viscoelastic models to experimental data. In: GALCIT Solid Mechanics Reports, vol. SM-61-23A. California Institute of Technology (1962)

Schapery, R.A.: Application of thermodynamics to thermomechanical, fracture, and birefringent phenomena in viscoelastic media. J. Appl. Phys. **35**, 1451–1465 (1964)

Schapery, R.A.: A method of viscoelastic stress analysis using elastic solutions. J. Franklin Inst. **279**, 268–289 (1965)

Schapery, R.A.: On the characterization of nonlinear viscoelastic materials. Polym. Eng. Sci. **9**, 295–310 (1969)

Schapery, R.A.: Nonlinear facture analysis of viscoelastic composite materials based on a generalized j integral theory. In: Akasak, K.K.T. (ed.) Proc. Japan-U.S. Conference Composite Materials, Tokyo (1981)

Tschoegl, N.W.: The Phenomenological Theory of Linear Viscoelastic Behavior: An Introduction. Springer, Berlin (2012)

Tschoegl, N.W., Knauss, W.G., Emri, I.: Poisson's ratio in linear viscoelasticity—a critical review. Mech. Time-Depend. Mater. **6**, 3–51 (2002)

Viktorova, I.: Description of the delayed fracture of inelastic materials taking temperature into account. Mech. Compos. Mater. **19**(1), 35–38 (1983)

Williams, M.L., Landel, R.F., Ferry, J.D.: The temperature dependence of relaxation mechanisms in amorphous polymers and other glass-forming liquids. J. Am. Chem. Soc. **77**, 3701–3707 (1955)